Pulse Design for Relaxation Adiabat-Shaped Targets in Inertial Fusion Implosions

Introduction

Controlling the seeds and the growth of Rayleigh–Taylor (RT) instability during the acceleration phase of imploding shells is crucial to the success of inertial confinement fusion (ICF). Since the RT growth is damped by the ablative flow off the shell's outer surface, target performances are greatly improved by target designs with enhanced ablation velocity. A significant increase in ablation velocity and shell stability can be achieved by shaping the entropy inside the shell. Following the standard ICF notation, we measure the entropy through the so-called "adiabat" defined as the ratio of the plasma pressure to the Fermi-degenerate DT pressure: $\alpha \equiv P(\text{Mb})/2.18\rho(\text{g/cc})^{5/3}$, where the pressure is given in megabars and the density in g/cc. The optimum adiabat shape in the shell consists of a profile that is monotonically decreasing from the outer to the inner surface as qualitatively shown in Fig. 101.8 on p. 14. Large adiabat values on the shell's outer surface increase the ablation velocity V_a, which follows a power law of the outer-surface adiabat $\alpha_{\text{out}}, [V_a \sim \alpha_{\text{out}}^{3/5}]$, while low adiabat values on the inner surface lead to improved ignition conditions and larger burn.[1–5] A more detailed history and target design implications of adiabat shaping can be found in the introduction of Ref. 6 by the same authors, which is devoted mostly to the adiabat shape induced by a strong decaying shock. Shaping by a decaying shock was introduced in Ref. 7 and requires a very strong prepulse aimed at launching a strong shock. This strong shock decays inside the shell shortly after the prepulse is turned off; the picket pulse is followed by the low-intensity foot of the main pulse. The decaying shock (DS) leaves behind a monotonically decreasing adiabat profile, which follows a power law of the mass coordinate

$$\alpha_{\text{DS}} = \alpha_{\text{inn}} \left(\frac{m_{\text{shell}}}{m} \right)^{\delta_{\text{DS}}}, \tag{1}$$

where m is the mass calculated from the outer surface, m_{shell} is the total shell mass, and α_{inn} is the adiabat on the shell's inner surface. The value of δ_{DS}, calculated in Ref. 6, is approximately independent of the prepulse characteristics. Without accounting for the effect of mass ablation, δ_{DS} is about 1.3.

If mass ablation is included, δ_{DS} varies between 1.06 and 1.13, depending on the prepulse duration.[6] Two-dimensional (2-D) simulations[7] of all-DT, OMEGA-size-capsule implosions have confirmed that DS adiabat targets exhibit significantly reduced RT growth on the ablation surface during the acceleration phase with respect to the flat-adiabat ones. Comparisons between flat- and shaped-adiabat targets are typically carried out by designing the flat- and shaped-adiabat pulses to generate identical adiabats on the shell's inner surface.

A different technique aimed at shaping the adiabat is the so-called shaping by relaxation (or RX shaping) first introduced in Ref. 8. The relaxation technique uses a less-energetic prepulse than the DS technique. The RX prepulse (Fig. 101.1) is used to launch a shock that may or may not decay inside the shell. In both cases, the prepulse is turned off before the prepulse shock reaches the shell's inner surface. Since the prepulse is followed by a complete power shutoff, the outer portion of the shell expands outward, generating a relaxed density profile while the prepulse shock travels inside the shell. The prepulse shock is not intended to greatly change the shell adiabat even though
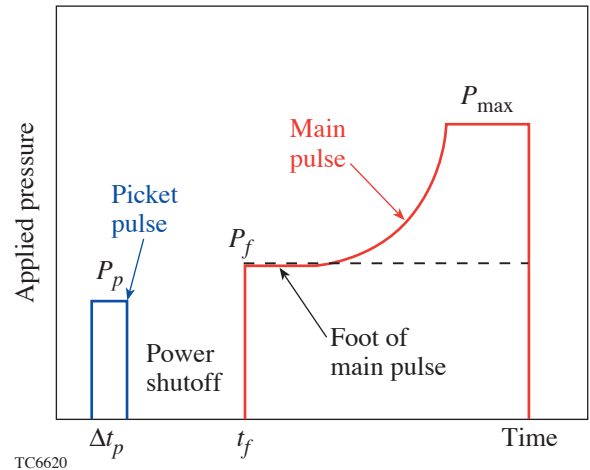

Figure 101.1
Typical pressure pulse for adiabat shaping by relaxation.

it may cause a significant adiabat modification. The main adiabat shaping occurs later in time when the foot of the main pulse starts and a strong shock travels up the relaxed density profile. The main shock first encounters the low-density portion of the relaxed profile, setting it on a very high adiabat. The adiabat develops a monotonically decreasing profile as a result of the increasing pre-shock density. Figures 101.2(a), 101.2(b), and 101.2(c) show three snapshots of the main shock propagation (m.s.) through a relaxed density profile. The density profile of an 85-μm-thick DT target is relaxed by a 60-ps, 13-Mb prepulse. The prepulse shock (p.s.) travels ahead of the main pulse shock. The latter is launched by a 15-Mb pressure applied at 1941 ps. The main shock launching time (or main pulse foot beginning time) is chosen in order to cause the main and prepulse shocks to merge on the shell's inner surface. A plot of the shaped-adiabat profile at shock breakout is shown in Fig. 101.2(d). Observe that the adiabat varies from about 2 on the inner surface to several tens on the outer surface. Two-dimensional (2-D) simulations[8–10] of OMEGA- and NIF-size-capsule implosions have confirmed that RX-shaped targets exhibit significantly reduced RT growth on the ablation surface during the acceleration phase with respect to the flat-adiabat ones.

The RX adiabat-shaping technique can be viewed as a two-step process: the prepulse and power shutoff are needed to generate the relaxed density profile, while the foot of the main pulse shapes the adiabat. Similarly to the DS shaping, the RX adiabat profile can be approximated with a power law of the mass coordinate

$$\alpha_{\mathrm{RX}} \simeq \alpha_{\mathrm{inn}} \left(\frac{m_{\mathrm{shell}}}{m} \right)^{\delta_{\mathrm{RX}}}, \qquad (2)$$

where δ_{RX} can be tailored between a minimum of zero (i.e., no shaping) to a maximum value of 2.4. This upper bound, which is well above the decaying shock value, can be achieved only for weak prepulses (either low-pressure or short-duration prepulses) and by neglecting the effects of mass ablation. For realistic prepulses and including the effect of ablation, the maximum RX power index is reduced to values in the range of 1.6 to 1.8, which is still significantly larger than the 1.1 of the decaying shock. Since the steeper RX adiabat profile leads to greater values of the outer-surface adiabat with respect to the DS adiabat shaping, one can conclude that the ablation velocity will be significantly higher in RX-shaped targets than DS-shaped targets. Furthermore, the tailoring of the adiabat steepness in RX shaping is beneficial to the control of the convective instability, which is driven by the finite entropy gradients inside the shell. This instability grows at a slower rate with respect to the Rayleigh–Taylor and does not seem to cause a significant distortion of the shell.[7,8]

Different adiabat-shaping techniques based on the tailoring of the radiation absorption in the target have also been proposed;[11–13] however, their implementation relies on manufacturing targets with a spatially varying atomic number, a technique that is difficult in cryogenic capsules. It has also been suggested[14] that some classified work on adiabat shaping was initiated in the 1980s by Verdon, Haan, and Tabak. This work
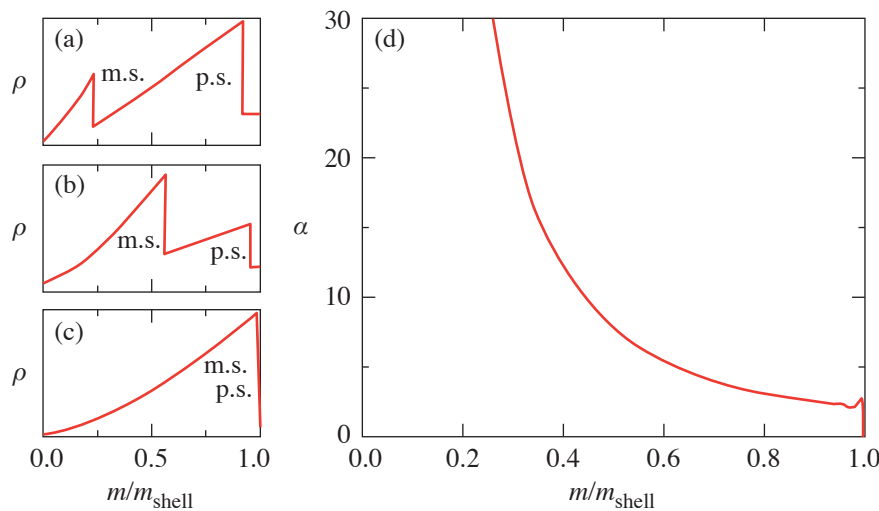

Figure 101.2
Snapshots [(a),(b), and (c)] of the density profiles at different stages of the main-shock and prepulse-shock propagation. The resulting adiabat profile left behind the main shock at breakout time is shown in (d).

TC6621

appears to be restricted, however, to the classified literature and was not accessible to Betti and Anderson (authors of the earlier published work[8] on RX shaping and co-authors of the current article). It is also important to clarify the role of earlier work[15] on the so-called "picket-fence" pulses and make a distinction between adiabat shaping and picket fence. The picket-fence pulse consists of a sequence of relatively short pulses that replace the standard isentropic continuous pulse. When plotted versus time, the laser power of such a sequence of short pulses (see Fig. 3 of Ref. 15) resembles a picket fence. Instead, both DS adiabat shaping and RX adiabat shaping make use of a single short pulse (i.e., the laser prepulse) followed by a continuous pulse. Thus, except for the prepulse, the adiabat-shaping pulses are essentially continuous. While a claim can be made that adiabat shaping and picket fence use some sort of picket pulse, it would be grossly inaccurate to think of the two techniques as equal or even similar. As stated in Ref. 15, the goal of the picket-fence pulse is to replace a continuous acceleration with an impulsive one. The rationale behind this clever idea is that the RT exponential growth turns into a sequence of linear-growth stages, thus reducing the overall growth factor (as long as the number of pickets is kept relatively low). On the contrary, adiabat shaping does not change the time evolution of the acceleration. Its primary effect is to increase the ablation velocity, thus enhancing the ablative stabilization of the RT instability. Though the physical basis and pulse design of a picket-fence pulse have little (if anything) in common with adiabat shaping, it is possible that some level of adiabat shaping may occur in picket-fence implosions due to the repeated decompressions between short pulses. Though this collateral effect was not considered in Ref. 15, it would be worth investigating the degree at which the adiabat is shaped in picket-fence implosions. It is also worth mentioning that the evolution of the laser power in Fig. 2 of Ref. 15 seems to point to a single prepulse followed by a continuous main pulse. While this pulse resembles an RX pulse, the authors of Ref. 15 do not address the possibility that adiabat shaping may occur.

Lastly, it is important to recognize that the presence of a laser prepulse could have significant consequences with regard to the level of laser imprinting. Laser imprinting is caused by the spatial nonuniformities of the laser intensity and is widely considered as the main seed for the short-wavelength RT instability in direct-drive implosions. It has been recently shown[16–18] that the level of imprinting can be significantly reduced by tailoring the initial target density with a monotonically increasing profile varying from a lower value on the outer surface to its maximum on the shell's inner surface. Since the

laser prepulse in RX adiabat shaping causes such a monotonically varying density profile, it is likely that RX shaping may also reduce the level of imprinting. Furthermore, it has been shown in Ref. 19 that, in the presence of a plastic (or other) coating on cryogenic capsules, the acceleration of the plastic layer against the cryogenic DT layer causes a brief exponential amplification of the imprinting level. Reference 19 also shows that this amplification can be reduced by using a sufficiently strong prepulse. Such an improvement of the imprinted nonuniformities requires a strong prepulse and may therefore be more effective in DS shaping than in RX shaping. Imprint reduction using prepulses has also been demonstrated by both simulation and experiment in single-layer targets made of aluminum.[20] While some encouraging results on the stability of RX-shaped capsule implosions have been obtained from 2-D simulations[8–10] and from experiments on plastic-shell implosions,[10] a more detailed 2-D analysis including the effect of RX shaping on imprinting as well as a complete description of the experiments carried out on the OMEGA laser system will be presented in a forthcoming publication.

In this article, we cite the results of the one-dimensional (1-D) hydrodynamic analysis of the relaxation adiabat profiles,[21,22] simplify them with power-law approximations, and compare them with decaying-shock-adiabat profiles and to simulations. Furthermore, we derive formulas for relaxation pulse design and discuss nonideal effects, such as mass ablation, on the adiabat profiles.

Summary of Previously Derived Adiabat Profiles

References 21 and 22 divide relaxation adiabat shaping designs into two categories: type 1, where the prepulse shock and rarefaction merge at the rear surface of the shell; and type 2, where the rarefaction merges with the prepulse shock within the shell. These two designs yield different adiabat profiles. An accurate description of the type-1 adiabat profile is well approximated by the following set of equations from Eqs. (75)–(77) and (46b), respectively, of Ref. 22:

$$S = S_{\text{inn}} \left(\frac{m_{\text{shell}}}{m} \right)^{\frac{2\gamma}{\gamma+1}} \frac{\chi(1)}{\chi\left(\frac{m}{m_{\text{shell}}}\right)}, \quad (3)$$

where

$$S_{\text{inn}} = \frac{(\gamma-1)^{2\gamma}}{\gamma\chi(1)(\gamma+1)^{2\gamma-1}} \frac{P_f}{\rho_0^\gamma} \quad (4)$$

is the entropy on the shell's inner surface and ρ_0 is the initial shell density. The function $\chi(x)$ represents the corrections due to the finite main shock strength

$$\chi(x) = \tilde{\rho}\left\{\frac{\gamma P_p \Theta(x)}{(\gamma+1)P_f}\left[\frac{x}{\sum(x)}\right]^{\frac{2\gamma}{\gamma+1}}\right\}^{\gamma} \frac{\Theta(x)}{\sum(x)^{\frac{2\gamma}{\gamma+1}}}, \quad (5)$$

$$\tilde{\rho}(\hat{\pi}) = \frac{1+\frac{\gamma-1}{\gamma+1}\hat{\pi}}{1+\frac{\gamma+1}{\gamma-1}\hat{\pi}} \simeq 1 - \frac{4\gamma}{\gamma^2-1}\hat{\pi} + \mathcal{O}(\hat{\pi}^2), \quad (6)$$

and where $\beta \simeq 2/(\gamma+1)$ and $\hat{\pi} = P_p/P_f$ is the ratio of the prepulse pressure to the pressure of the foot of the main pulse.

The type-2 adiabat profiles are steeper than the type-1 profiles and can be approximated as

$$S(m) \simeq \frac{\omega_* P_f}{\rho_M^{\gamma}}\left(\frac{z_{\text{shell}}}{z}\right)^{\gamma\mu}[1+D(z)(z-1)]\hat{s}(z), \quad (7)$$

$$\hat{s}(z) = \frac{\left\{1 - \phi \hat{m}_*^{\phi}\sqrt{\frac{2(\gamma-1)}{(\gamma+1)\omega_*}\frac{P_p}{P_f}}[\sigma(z_{\text{shell}})-\sigma(z)]\right\}^{\frac{\gamma\mu}{\phi}}}{\left\{\tilde{\rho}\left[\frac{P_p}{\omega_* P_f}\frac{\hat{m}_*^{\mu\gamma}z^{\mu\gamma-\delta}}{1+D_0(z)(z-1)}\right]\right\}^{\gamma}}, \quad (8)$$

$$\omega_* = \omega_0\left[1 - \frac{2\beta(\gamma+2)}{3(2-\beta)}\sqrt{\frac{2\gamma P_p}{\omega_0(\gamma+1)P_f}}\left(\frac{m_*}{m_{\text{rf}}^0}\right)^{1-\frac{\beta}{2}}\right], \quad (9)$$

where $D(x) = D_0(x) + D_1(x)$,

$$D_0(x) = \frac{2(x^{\mu}-1) + \mu(x-3)(x-1) - \mu^2(x-1)^2}{(\mu-2)(\mu-1)(x-1)^3}, \quad (10)$$

$$D_1(x) = -\mu\sqrt{\frac{\gamma-1}{\gamma+1}\frac{P_p}{\omega_* P_f}}\frac{\hat{m}_*^{\phi}\left(z_s^M\right)^{\mu}}{\left(z_s^M-1\right)^3}$$

$$\times \int_1^{z_s^M}\sqrt{\frac{(x-1)^4 + D_0(x)(x-1)^5}{x^{3\mu}}}\,dx, \quad (11)$$

and $\tilde{\rho}(x)$ is given by Eq. (6). These formulas are derived in Ref. 22 as Eqs. (100a), (100b), (90), (82), and (94), respectively.

In practical terms, these formulas for the relaxation-adiabat profiles are cumbersome and provide no intuitive comparison with decaying-shock-adiabat profiles. Therefore, in the following section, simple power-law approximations to these formulas are calculated.

Simplified Formulas for RX Adiabat Shapes and Comparison with DS Shapes

The theoretical results derived in the previous section can be simplified by fitting the adiabat shapes with a simple power law in the mass coordinate. It has been shown in Ref. 6 that the power-law approximation works extremely well for the adiabat shape left behind by a decaying shock (DS shaping). In an ideal fluid with adiabatic index $\gamma = 5/3$ and neglecting the effects of mass ablation, the adiabat profile left behind by a decaying shock follows the power law $\alpha_{\text{DS}} \sim 1/m^{1.315}$ for $m_* < m < 10\,m_*$. It is worth mentioning that the power index is approximately independent of the prepulse characteristics.

Adiabat shaping by relaxation leads to a tunable adiabat profile ranging from a rather shallow profile for RX shaping of type 1 to a steeper profile with RX shaping of type 2. In the case of RX shaping of type 1, the shaping function given in Eqs. (3)–(5) can be well approximated for $\gamma = 5/3$ by the following power law of the mass coordinate:

$$\alpha_{\text{RX1}} = \alpha_{\text{inn}}^{\text{RX1}}\left(\frac{m_{\text{shell}}}{m}\right)^{\delta_{\text{RX1}}}, \quad (12)$$

where the power index δ_{RX1} and the inner-surface adiabat $\alpha_{\text{inn}}^{\text{RX1}}$ are functions of prepulse/main-pulse pressure ratio $r_p \equiv P_p/P_f$. A straightforward numerical fit leads to the following fitting functions:

$$\alpha_{\text{inn}}^{\text{RX1}} \simeq 7.2 \cdot 10^{-3} \frac{P_f(\text{Mb})}{\rho_0(\text{g/cc})^{5/3}}$$

$$\times \left(1 - 1.12 r_p^{0.52} + 6.54 r_p^{1.15}\right), \qquad (13)$$

$$\delta_{\text{RX1}} \simeq 1.25 - 4.14 r_p^{0.95} + 3.05 r_p^{1.61}, \qquad (14)$$

where ρ_0 is the initial shell density. These approximate formulas have been derived by fitting the adiabat profile over the range $0.2 < m/m_{\text{shell}} < 1$ and $0 < r_p < 0.75$. Observe that the steepest profile of the first kind behaves as $1/m^{1.25}$ and occurs for $r_p \to 0$. For typical values of prepulse- to foot-pressure ratios in the range $0.05 < r_p < 0.2$, the power index of the adiabat profile is within the range 0.60 to 1.04, which is well below the decaying shock value of 1.315, thus indicating that the DS shaping leads to notably steeper adiabat profiles than the relaxation method of type 1.

In RX shaping of type 2, the adiabat profile left behind by the main shock [Eqs. (7)–(11)] can also be approximated by a power law of the mass coordinate

$$\alpha_{\text{RX2}} \simeq \alpha_{\text{inn}}^{\text{RX2}} \left(\frac{m_{\text{shell}}}{m}\right)^{\delta_{\text{RX2}}}, \qquad (15)$$

where

$$\alpha_{\text{inn}}^{\text{RX2}} = 2.46 \cdot 10^{-2} \frac{P_f(\text{Mb})}{\rho_0(\text{g/cc})^{5/3}}$$

$$\times \left(1.19 + 1.76 r_p^{0.8} \hat{m}_*^{2.15} - 1.11 \hat{m}_*^{0.25}\right), \qquad (16)$$

$$\delta_{\text{RX2}} \simeq 2.105 - 3.469 r_p^{0.62} \hat{m}_*^{1.31}, \qquad (17)$$

and where $m_* = 2.09 \Delta t_p \sqrt{P_p \rho_0}$, Δt_p is the prepulse duration, and $m_{\text{shell}} = \rho_0 d_0$ (d_0 is the initial shell thickness). It is important to emphasize that Eqs. (15)–(17) have been derived by fitting Eqs. (7)–(11) for an ideal fluid (no ablation) with $\gamma = 5/3$ and pulse/target characteristics satisfying $0.2 < r_p < 1$ and $0.05 < \hat{m}_* < 0.4$. It is also interesting to note that the power

index δ_{RX2} is maximum for short prepulses and/or weak prepulses $(\hat{m}_* \ll 1, r_p \ll 1)$. For $\hat{m}_* \to 0$, the RX adiabat profile of Eqs. (7)–(11) reduces to a power law with a power index $\delta_{\text{RX2}} \simeq 2.4$, well above the power index of the decaying shock shaping $\delta_{\text{DS}} \simeq 1.315$. However, the ratio m_*/m_{shell} cannot be arbitrarily small for RX shaping since the pressure behind the prepulse shock at its arrival on the inner surface, which is approximately $P_p \hat{m}_*^{1.3}$, must be large enough to keep the prepulse shock in the strong shock regime and to ionize the target material. Typical values of δ_{RX2} are mostly in the range 1.7 to 2.0, which is still significantly larger than the 1.315 of the decaying shock.

It has been shown in Ref. 6 that ablation causes the adiabat profile induced by a decaying shock to become shallower. This is because the shock decays more slowly due to the residual ablation pressure and the fact that the supporting pressure moves closer to the shock. In the relaxation method of type 2, the relaxed density profile is produced by a decaying shock driven by the pressure prepulse. Since ablation causes a slow-down of the shock decay, it follows that the relaxed profile is "less relaxed" because of ablation. Therefore, the adiabat shape induced by the main shock is less steep than in the ideal case without ablation. Typical ablation-induced reductions of the adiabat profile power index δ_{RX} are small (of the order of 10%) and lead to a power index in the range $\delta_{\text{RX2}} \simeq 1.6$ to 1.8.

Pulse Design

To induce the desired adiabat profile, one needs to design the appropriate applied pressure pulse. The pressure pulse (Fig. 101.1) consists of a constant prepulse of pressure P_p and duration Δt_p followed by a main pulse of pressure P_f applied at time t_f. Typically, the pulse is designed to induce the desired value of the inner-surface adiabat α_{inn}. The latter is a design parameter that needs to satisfy the one-dimensional ignition and gain requirements of the implosion. Another design constraint is the merging of the prepulse and main shocks on the shell's inner surface. This is required in order to keep the adiabat profile monotonically decreasing. For the relaxation pulse of type 1, another requirement is the merging of the rarefaction wave with the prepulse and main shocks on the shell's inner surface. Therefore, given the four pulse parameters (P_p, P_f, Δt_p, and t_f), the type-1 relaxation has three constraints and one free parameter, while the type-2 relaxation has two constraints and two free parameters. Since different pulse parameters lead to different adiabat decay rates, another design parameter can be identified as the adiabat profile's spatial decay rate. By approximating the adiabat profile with a power law $S \sim 1/m^\Delta$, the power index Δ defines the decay

rate and can be assigned as a design parameter (within the appropriate limits), thus further reducing the degrees of freedom. Furthermore, technical limits on the prepulse and foot pressure as well as prepulse duration are imposed by the pulse-shaping capabilities of a given laser system. Such limitations are not discussed in this article but need to be taken into account when designing an adiabat-shaping pulse. In this section we proceed to determine the relevant parameters needed to design a pressure pulse for RX adiabat shaping.

1. Pulse Design for RX Shaping of Type 1

The pulse design for a relaxation shaping of type 1 is highly constrained since the prepulse shock, the rarefaction wave, and the main shock must all merge on the shell's rear surface. By combining the Hugoniot condition on the shock velocity

$$\dot{m}_s^M = \sqrt{(\gamma+1)P_{ps}\rho_{bs}/2},$$

the type-1 post-main-shock pressure from Eqs. (73) of Ref. 22

$$P_{ps}^M = P_M/\Theta(\eta_s), \tag{18a}$$

$$\Theta(x) = 1 + \frac{2\beta(\gamma+2)}{3(2-\beta)}\sqrt{\frac{2\gamma P_p}{(\gamma+1)P_M}}x^{1-\frac{\beta}{2}}, \tag{18b}$$

and the pre-shock density $\rho_{bs}^M = \rho_p\left(m_s^M/m_{rf}\right)^\beta$, with $m_{rf} = m_{shell}\tau$ and

$$\tau = t/\Delta t_*, \tag{19}$$

$$\Delta t_* = \frac{\Delta t_p}{\sqrt{2\gamma/(\gamma-1)}-1} \tag{20}$$

from Eqs. (12)–(13) of Ref. 22, one can easily derive the following ordinary differential equation for the main-shock propagation:

$$\frac{d\eta_s^M}{d\tau} = \frac{\gamma+1}{\gamma}\sqrt{\frac{P_f}{2P_p\Theta(\eta_s^M)}}\left(\frac{\eta_s^M}{\tau}\right)^\beta, \tag{21}$$

where $\eta_s^M = m/m_{shell}$ and Θ is derived from Eq. (18b) for $\beta = 2/(\gamma+1)$, leading to

$$\Theta = 1 + \frac{2(\gamma+2)}{3(\gamma+1)}\sqrt{\frac{2P_p}{P_f}}\left(\eta_s^M\right)^{\frac{\gamma}{\gamma+1}}. \tag{22}$$

A straightforward integration of Eq. (21) for $\eta_s^M \in [0,1]$ and $\tau \in [\tau_f, 1]$ leads to the following expression for the beginning time of the foot pulse:

$$t_f = \Delta t_p + \tau_f \Delta t_*, \tag{23a}$$

$$\tau_f = \left\{1 - \frac{\gamma}{\gamma+1}\sqrt{\frac{2P_p}{P_f}}\left[1 + \frac{\gamma+2}{6(\gamma+1)}\sqrt{\frac{2P_p}{P_f}}\right]\right\}^{\frac{\gamma+1}{\gamma}}, \tag{23b}$$

where Δt_* is proportional to the prepulse duration Δt_p through Eq. (20). The main-shock breakout time coincides with the prepulse shock and rarefaction-wave breakout time on the inner surface given by the simple relation

$$t_{b.o.} = \Delta t_p + \Delta t_*. \tag{24}$$

The inner-surface adiabat induced by such a pulse is given by Eq. (13) and is primarily dependent on the foot pressure. If the inner-surface adiabat is an assigned design parameter, then Eq. (13) is used to constrain the foot pressure P_f. Note that the prepulse pressure and duration are related by the rarefaction wave/prepulse shock overtaking time, $m_* = m_{shell} \equiv \rho_0 d_0$ or

$$\Delta t_p \sqrt{P_p} = \sqrt{\rho_0} d_0 \frac{\sqrt{2\gamma}-\sqrt{\gamma-1}}{\sqrt{\gamma(\gamma+1)}}. \tag{25}$$

It follows that, for an assigned prepulse pressure (or duration) and inner-surface adiabat, there is only one foot pressure that would shape the adiabat with a profile of type 1 [Eqs. (12)–(14)]. As an example, we consider a 100-μm-thick DT shell ($\rho_0 = 0.25$ g/cc, $d_0 = 100$ μm) and design a type-1 RX shaping pulse using a prepulse given by $P_p = 5$ Mb, requiring an inner-surface adiabat $\alpha_{inn} \simeq 3$. Equation (25) yields a prepulse duration of $\Delta t_p \simeq 1070$ ps, while the foot pressure can be determined from Eq. (13) by setting $\alpha_{inn} = 3$. A straightforward calculation yields the foot pressure $P_f \simeq 29.7$ Mb. The foot pressure is applied at the time t_f obtained from Eq. (23),

yielding $t_f \simeq 1442$ ps. The shock-breakout time on the inner surface is given by Eq. (24), yielding $t_{b.o.} \simeq 1936$ ps. The corresponding adiabat profile has an approximate power-law behavior [Eq. (12)] with power index $\delta_{RX1} \simeq 0.67$ given by Eq. (14). Observe that Eq. (23b) suggests that a critical value of P_p/P_f exists that makes $\tau_f = 0$. Though such a critical value is not accurately predicted by the weak prepulse theory $(P_p \ll P_f)$ derived in this article, it is intuitive that an upper limit in the ratio P_p/P_f must exist in the design of a relaxation pulse of the first kind. Indeed, for a given prepulse pressure, the foot pressure must be sufficiently large to cause the main shock to catch the prepulse shock on the shell's rear surface.

2. Pulse Design Shaping for RX Shaping of Type 2

The shock-merging constraint requires that both the prepulse and the main shock merge at the rear surface. The prepulse-shock breakout time ($t_{b.o.}$) on the rear surface can be easily obtained from Eq. (32) of Ref. 22,

$$z_s^p(\tau) = \left[1 + \left(1 + \frac{\delta}{2}\right)\sqrt{\frac{\gamma - 1}{2\gamma}}(\tau - 1)\right]^{\frac{2}{2+\delta}}, \qquad (26)$$

by setting $z_s^p = z_{shell} \equiv m_{shell}/m_*$, thus leading to

$$t_{b.o.} = \Delta t_p + \Delta t_* \tau_{b.o.}, \qquad (27a)$$

$$\tau_{b.o.} \equiv 1 + \frac{2}{2 + \delta}\sqrt{\frac{2\gamma}{\gamma - 1}}\left[z_{shell}^{(2+\delta)/2} - 1\right], \qquad (27b)$$

where Δt_* is given in Eq. (20) and m_* in Eq. (14) of Ref. 22:

$$m_* = \Delta t_* \rho_p a_p = \Delta t_* \sqrt{\gamma P_p \rho_p}. \qquad (28)$$

The main shock must also arrive on the rear surface at time $t_{b.o.}$ by traveling through the $m > m_*$ and $m < m_*$ regions. The main shock's traveling time through the $m > m_*$ region can be easily derived by integrating Eq. (91) of Ref. 22:

$$\dot{m}_s^M = \sqrt{\frac{\gamma - 1}{2}\omega_* P_f \rho_M \left(\frac{m_s^M}{m_s^p}\right)^\mu \left[1 + D(z_s^M)(z_s^M - 1)\right]}. \qquad (29)$$

A straightforward manipulation yields the following traveling time:

$$\Delta t_{m>m_*}^M = \Delta t_* \Delta \tau_{m>m_*}^M, \qquad (30a)$$

where

$$\Delta \tau_{m>m_*}^M = \sqrt{\frac{2\gamma}{\gamma + 1}\frac{P_p}{\omega_* P_f}}$$

$$\times \int_1^{z_{shell}} \frac{(z_s^p)^{\mu/2} dz_s^M}{\sqrt{(z_s^M)^\mu \left[1 + D(z_s^M)(z_s^M - 1)\right]}}, \qquad (30b)$$

z_s^p is a function of z_s^M [Eqs. (96)–(97) of Ref. 22],

$$(z_s^p)^\phi - z_{shell}^\phi = \phi\sqrt{\frac{2(\gamma - 1)}{\gamma + 1}\frac{P_p}{\omega_* P_f}}\left[\sigma(z_s^M) - \sigma(z_{shell})\right], \qquad (31)$$

where $z_s^p = m_s^p/m_*$, $z_{shell} = z_{shell} = m_{shell}/m_*$, and

$$\sigma(\xi) = \sqrt{\frac{(\mu - 2)\xi^{1-\mu} - (\mu - 1)\xi^{2-\mu} + 1}{(\mu - 2)(\mu - 1)}}, \qquad (32)$$

and $D(x)$, ω_* are given in Eqs. (10), (11), and (9). It follows that the time when the main shock is at $m = m_*$ is $t_{m=m_*}^M = \Delta t_p + \Delta t_* \tau_{m=m_*}$, where $\tau_{m=m_*} \equiv \tau_{b.o.} - \Delta \tau_{m>m_*}^M$. Before arriving at m_*, the main shock travels through the region $0 < m < m_*$, where the density profile is given by Eq. (44) of Ref. 22,

$$\rho(z < 1) \approx \rho_p \left(\frac{z}{\tau}\right)^\beta = \rho_p \left(\frac{m}{m_{rf}}\right)^\beta, \qquad (33)$$

and the post-shock pressure follows Eq. (18) with $\eta = m_s^M/m_{rf}^0$ and m_{rf}^0 given in Eq. (89) of Ref. 22,

$$m_{\mathrm{rf}}^0 = m_* \left\{ 1 + \frac{2}{2+\delta} \sqrt{\frac{2\gamma}{\gamma-1}} \left[z_{\mathrm{shell}}^{(2+\delta)/2} - 1 \right] \right\}. \tag{34}$$

The shock-evolution equation is given by the Hugoniot condition [Eq. (10) of Ref. 22]

$$\dot{m}_s = \sqrt{\frac{(\gamma+1)}{2} \left[P_{\mathrm{ps}} \rho_{\mathrm{bs}} \right]_{m_s}}, \tag{35}$$

which can be integrated between the main-shock launching time (or main-pulse foot beginning time t_f) and the arrival time at $m = m_*$. A short calculation yields the launching time

$$t_f = \Delta t_* \tau_f + \Delta t_p, \tag{36a}$$

$$\tau_f \equiv \left[\tau_{m=m_*}^{(2-\beta)/2} - \left(1 - \frac{\beta}{2} \right) \theta \sqrt{\frac{2\gamma}{\gamma+1} \frac{P_p}{\omega_0 P_f}} \right]^{\frac{2}{2-\beta}}, \tag{36b}$$

where

$$\theta = \int_0^1 dx \frac{1}{\chi^{\beta/2}}$$

$$\times \left[1 - \frac{2\beta(\gamma+2)}{3(2-\beta)} \sqrt{\frac{2\gamma P_p}{(\gamma+1)\omega_0 P_f}} \left(\frac{xm_*}{m_{\mathrm{rf}}^0} \right)^{\frac{2-\beta}{\beta}} \right]^{-\frac{1}{2}}. \tag{36c}$$

Observe that Eqs. 36 provide the beginning time of the foot of the main pulse once the prepulse pressure P_p, foot pressure P_f, and prepulse duration Δt_p are assigned. The time t_f is derived by timing the prepulse and main shock so that they merge on the shell's inner surface. As an example, we consider a 100-μm-thick DT shell ($\rho_0 = 0.25$ g/cc, $d_0 = 100$ μm) and design a type-2 RX shaping pulse using a $P_p = 18$ Mb, $\Delta t_p = 100$-ps prepulse and requiring an inner-surface adiabat $\alpha_{\mathrm{inn}} \simeq 3$. Using the definition $m_{\mathrm{shell}} = \rho_0 d_0$ and Eqs. (20) and (28) to find m_*, one can easily compute the parameter $\hat{m}_* = 0.177$. The foot pressure can be determined by using $\alpha_{\mathrm{inn}} = 3$ into Eq. (16), yielding $P_f \simeq 24$ Mb. The time when the foot pressure is applied can be computed from Eqs. (36) using $\gamma = 5/3$, $\omega_0 \simeq 1.5$, and $\beta = 0.75$, leading to $t_f = 1256$ ps. The shocks' breakout/merging time is determined through Eqs. (27), leading to $t_{\mathrm{b.o.}} = 1993$ ps. The corresponding adiabat profile has an

approximate power-law behavior [Eq. (15)] with power index $\delta_{\mathrm{RX2}} \simeq 1.80$, which is significantly larger than in the case of the decaying-shock shaping.

It is important to recognize that typical laser pulses are designed so that the laser power reaches its peak at shock breakout. The corresponding laser pressure starts from the foot level (P_f) and increases monotonically to its maximum value $P_{\max}$ (Fig. 101.1). The laser power (and pressure) is raised at a low-enough rate to avoid strengthening the main shock and to prevent increasing the adiabat after the main shock. Since the resulting adiabat shape is set by the main shock driven by P_f, the theory derived in this article is valid for realistic ICF pulses with a laser-power raise after the foot (Fig. 101.1).

This concludes the analysis of the pulse design. A detailed comparison of the adiabat shapes and pulse-design parameters with the results of numerical simulation is carried out in the next section.
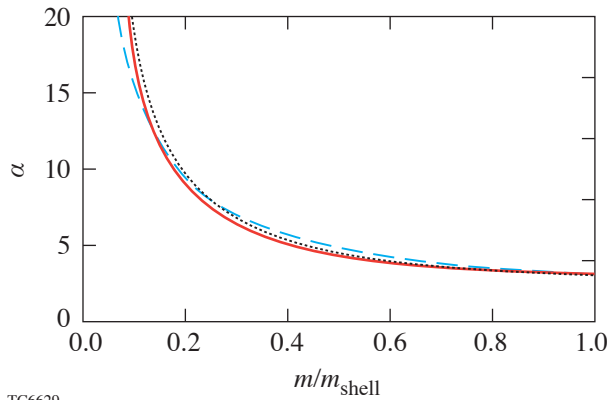
Comparison with Simulations

The results of the analytic theory derived in this article are compared to the numerical results calculated by a one-dimensional Lagrangian hydrodynamics code, using ideal gas equation of state and an imposed pressure boundary condition to simulate the relaxation drive pulses. We have chosen the case of $\alpha_{\mathrm{inn}} = 3$ as a case of interest, where adiabat shaping is expected to demonstrate significantly improved performance and to constrain our capsule and pulse designs to such as would be implementable on the OMEGA laser system.

Using the pulse-design formulas given in the **Pulse Design for RX Shaping of Type 1** section (p. 6), a type-1 RX pulse shape was designed for a typical OMEGA cryogenic capsule of density $\rho_0 = 0.25$ g/cm^3 and thickness $d_0 = 100$ μm using the parameters described in the example on pp. 6–7: $P_p = 5$ Mb, $\Delta t_p = 1070$ ps, $P_f = 29.7$ Mb, and $t_f = 1442$ ps. The shocks' breakout time is $t_{\mathrm{b.o.}} = 1936$ ps, and the resulting adiabat shape can be approximated with the power law $\alpha \simeq 3.04 (m_{\mathrm{shell}}/m)^{0.67}$. The pulse parameters have been used as input to the one-dimensional Lagrangian code that solves the equation of motion over a mesh of 2000 grid points. Figure 101.3 compares the adiabat profiles from the numerical simulation (solid curve) with the power-law approximation (dashed curve) and the full analytic formula in Eqs. (3)–(5) (dotted curve). Observe that the theoretical pulse parameters described on pp. 6–7 produce a monotonically decreasing adiabat profile with an inner-surface adiabat of about $\alpha_{\mathrm{inn}} \simeq 3$. Furthermore, the simulated adiabat profile compares favorably with the full
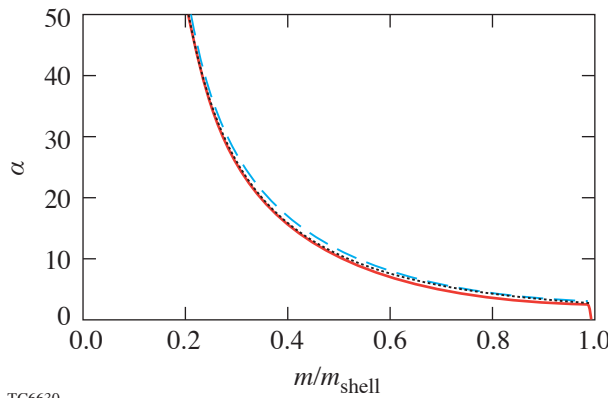
analytic formula as well as the power-law approximation described in the **Simplified Formulas for RX Adiabat Shapes and Comparison with DS Shapes** section (p. 4) for type-1 relaxation.

Similarly, a type-2 RX pulse shape is designed in the **Pulse Design for RX Shaping of Type 2** section (p. 7) for the same target with $\alpha_{inn} = 3$. The pulse parameters shown on p. 8 are $P_p = 18$ Mb, $P_f = 24$ Mb, $\Delta t_p = 100$ ps, and $t_f = 1256$ ps. The shocks' breakout time is $t_{b.o.} = 1993$ ps, and the adiabat profile can be approximated with the power law $\alpha \simeq 3.0\left(m_{shell}/m\right)^{1.8}$. Figure 101.4 compares the adiabat profiles from the numerical simulation (solid curve) with the power-law approximation

TC6629

Figure 101.3

A comparison of the simulated adiabat shape of type 1 (solid) with the full analytic formula [Eqs. (3)–(5)] (dotted) and the power-law approximation [Eqs. (12)–(14)] (dashed).

TC6630

Figure 101.4

A comparison of the simulated adiabat shape of type 2 (solid) with the full analytic formula [Eqs. (7)–(11)] (dotted) and the power-law approximation [Eqs. (15)–(17)] (dashed).

(dashed curve) and the full analytic formula in Eqs. (7)–(11) (dotted curve). Observe that the theoretical pulse parameters (p. 8) induce a monotonically decreasing adiabat profile with an inner-surface adiabat of about $\alpha_{inn} \simeq 3$. Even in this case, the simulated adiabat profile compares favorably with both the full analytic formula as well as the power-law approximation for type-2 relaxation.

Nonideal Effects on RX Adiabat Shaping

In realistic ICF implosions, quantifying the adiabat profile generated in a relaxation-design capsule is further complicated by other physical processes and constraints, such as radiation, thermal conduction, mass ablation, laser absorption and laser system constraints, realistic equations of state (EOS's), and spherical convergence. Radiation and thermal conduction effects may invalidate the assumption of isentropic flow away from the shocks. Mass ablation alters the position where the laser-induced shocks are launched and therefore affects the shock timing. In typical pulse designs, the laser-absorption histories, and hence applied pressure histories, are not constant over the duration of either the prepulse or the foot, as has been assumed in the previous analysis. Realistic EOS's yield different results for compressibility, shock and rarefaction speeds, and post-shock flow velocity than the ideal-gas approximation. A thorough theoretical treatment of these processes is beyond the scope of this article; however, an attempt is made here to quantify their effects on the shell's adiabat profile through simple reasoning and simulation.

In ICF capsules, the radiation emitted from the hot coronal plasma can penetrate the shell, heating the dense shell material up to a significant depth. This inevitably causes a "natural" shaping of the adiabat near the ablation front,[11–13] even when the laser pulse is designed to induce a flat adiabat. This effect may indeed be noticeable for capsules with high or moderate average atomic number, e.g., polystyrene plastic[23] (CH, $\langle Z \rangle = 3.5$). However, for the hydrogenic capsules ($Z = 1$) of interest for direct-drive ICF, the radiation shaping is typically negligible when compared with the laser-induced shaping discussed here.

Thermal conduction plays an essential role in ICF capsule implosions since the heat conducted from the laser-absorption region to the ablation surfaces determines the ablation pressure. At the ablation surface, the shell material absorbs heat rapidly, raising its adiabat quickly as it ablates off the shell. Once this shell material has been ablated, however, its adiabat is no longer relevant to the capsule stability since the ablation velocity is determined only by the local value of the adiabat at

the ablation surface. Furthermore, the contribution of heat conduction to the adiabat in the bulk of the shell is very small compared to the shock-induced adiabat since both the temperature and temperature gradients are small in the unablated shell. Therefore, thermal conduction effects on the adiabat profile (with the exception of mass ablation) may also be neglected.

Mass ablation occurs during the prepulse as well as the foot of the main pulse. While the mass ablated during the prepulse is negligible, a significant fraction ranging from 20% to 30% of the total shell mass is ablated during the foot of the main pulse. Since the mass m_* undertaken by the rarefaction wave before the interaction with the prepulse shock is small in type-2 adiabat shaping, the ablated mass m_{abl} often exceeds m_*. When this happens, the foot-pressure amplification through the region $0 < m < m_*$ is eliminated. In the absence of mass ablation, the applied foot pressure is amplified from P_f at $m = 0$ to $\omega_* P_f$ at m_*, where $\omega_* \approx 1.5$ is given in Eq. (9). If the mass m_* is quickly removed by mass ablation during the foot, then the main shock is launched with the pressure P_f instead of $\omega_* P_f$. Therefore, the validity of Eqs. (15)–(17) for the design of type-2 adiabat shaping can be easily extended to the ablative case by replacing the applied pressure P_f with $P_f/\omega_* \approx P_f/1.5$.

When dealing with thick cryogenic targets, spherical convergence effects should also be taken into account for an accurate estimate of the adiabat shapes. They can be easily included by replacing the areal mass coordinate m with the total mass coordinate $m^{sph} = \int_0^{\bar{r}} \bar{r}'^2 \rho(\bar{r}',0) d\bar{r}'$. This requires a redefinition of m_* as follows:

$$m_*^{sph} = \frac{\rho_0}{3}\left(R_{out}^3 - R_*^3\right),$$

where R_{out} is the initial outer radius of the shell and

$$R_*^{sph} = \sqrt{4P_p/3\rho_0}\left(\Delta t_p + \Delta t_*\right)$$

is the radial coordinate of the rarefaction–shock merging.

To quantitatively account for all these effects, simulations were performed using *LILAC*,[24] a 1-D Lagrangian ICF code. The *LILAC* simulations used *SESAME* EOS in a spherical geometry, while modeling laser absorption by ray trace and inverse bremsstrahlung, thermal conduction using a flux-limited local thermodynamic equilibrium treatment, and radiation transport using multigroup diffusion. The target is an 85-μm-thick, solid-DT shell. The laser pulse, designed in

accordance with pulse-shaping capabilities of the OMEGA laser system,[25] consists of an 80-ps, 15-TW square prepulse, with a finite ramp-up and ramp-down in intensity, followed by a 7-TW foot with finite ramp-up launched at about 950 ps. The average prepulse pressure found by *LILAC* is 23 Mb. The ablation pressure of the foot pulse at the time of shock generation is approximately 34 Mb. The resulting adiabat profile is shown in Fig. 101.5 (solid) and compared with the prediction of Eqs. (15)–(17) (dashed), including the above modifications, indicating good agreement between theory and simulation. Note that the optimal foot-pulse turn-on time predicted by theory is 800 ps, whereas the value in simulation was 950 ps, indicating that some retuning of the pulse was necessary.
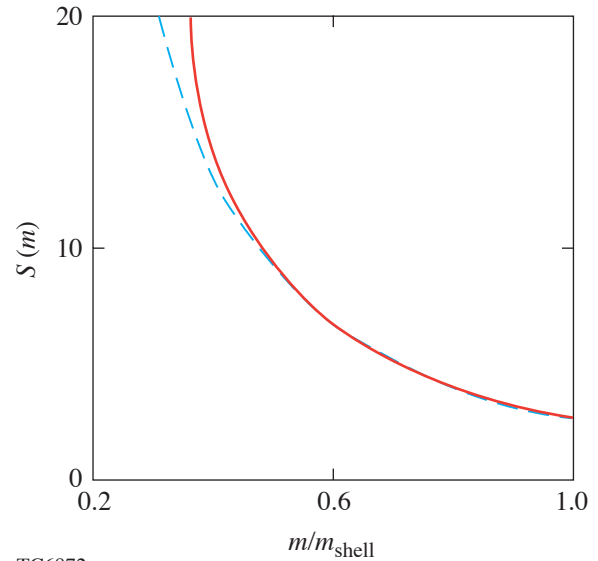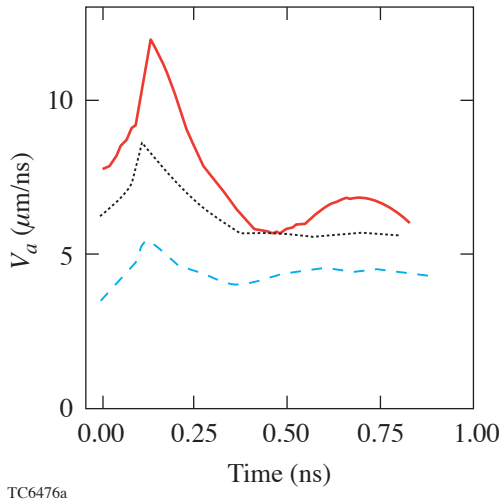

TC6872

Figure 101.5
A comparison of the simulated adiabat shape predicted by *LILAC* (solid) with the analytic formula [Eqs. (15)–(17)] (dashed) for an OMEGA-scale design.

To estimate the increase in ablation velocity, it is important to recognize that in realistic ICF implosions, a significant fraction of the target material is ablated off during the foot of the laser pulse. For an RX pulse shape, about 20% to 30% of the target mass is ablated before the shock-breakout time, thus causing the shell's outer surface to shift inward. The shell acceleration starts shortly after the shock-breakout time when the laser power reaches its peak. The relevant outer-surface adiabat determining the ablation velocity is the adiabat at the ablation front, which moves deeper inside the target as more mass is ablated off. In mass coordinates, the ablation-front position is equal to the amount of mass ablated, $m_a(t)$. It follows that the ablation velocity for a shaped-adiabat implosion is determined by the following simple scaling law:
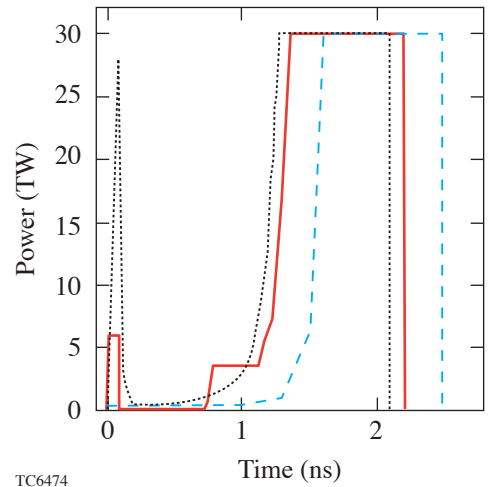
$$V_a^{\text{shaped}} \simeq V_a^{\text{flat}} \left(\frac{m_{\text{shell}}}{m_a(t)} \right)^{\frac{3}{5}\delta}, \qquad (37)$$

where V_a^{flat} is the ablation velocity for a flat-adiabat implosion with $\alpha = \alpha_{\text{inn}}$ and δ equal to δ_{RX1}, δ_{RX2}, or δ_{DS}, depending on the shaping method. During the acceleration phase, V_a is maximum at the beginning [low $m_a(t)$] and decreases in time as more mass is ablated and $m_a(t)$ increases. At the beginning of the acceleration phase when $m_a \sim 0.3\, m_{\text{shell}}$, the shaped-adiabat ablation velocity is roughly 2 times the flat-adiabat value for the decaying-shock shaping ($\delta_{\text{DS}} \simeq 1.1$), about 1.5 times V_a^{flat} for type-1 RX shaping ($\delta_{\text{RX1}} \sim 0.7$), and over 3 times V_a^{flat} for type-2 RX shaping ($\delta_{\text{RX2}} \sim 1.6$ to 1.8). Figure 101.6 shows the time evolution of the ablation velocities computed by *LILAC* for a typical OMEGA-size cryogenic DT shell of 85-μm thickness and 345-μm inner radius. The three curves represent the three pulse designs: flat adiabat with $\alpha = 3$ (dashed), shaped adiabat by decaying shock (dotted), and shaped adiabat by RX-2 shaping (solid). The corresponding laser time histories are shown in Fig. 101.7, and the time axis in Fig. 101.6 is adjusted to fit the different acceleration phases (i.e., maximum laser power intervals) of the three designs. Observe that the RX-2 design leads to the largest ablation velocity, approaching 3 times the flat-adiabat value at the beginning of the acceleration phase.

TC6474

Figure 101.7
Laser pulse for a flat $\alpha = 3$ design (dashed), a decaying-shock design (dotted), and a type-2 relaxation design (solid) of comparable 1-D performance.

Conclusions

Analytic forms of the relaxation adiabat shapes have been derived for two cases: type 1, where the prepulse is long enough that the rarefaction wave catches the prepulse shock at the shell's inner surface; and type 2, the case of short prepulses, where the rarefaction wave/shock interaction occurs inside the shell. The analytic relaxation adiabat profiles derived here are in excellent agreement with simulations. Results indicate that the adiabat profiles for both type-1 and type-2 designs are well approximated by a power law for ICF-relevant values of the prepulse to main-pulse pressure ratio. The power-law indices for RX designs have been shown to be highly tunable, giving the possibility for tailoring adiabat profiles to desired design specifications. The type-2 relaxation designs also allow for power-law indices, which are substantially higher than those generated by decaying-shock designs (see Ref. 6), resulting in the possibility of higher ablation velocities and higher RT mitigation in RX designs, while maintaining similar one-dimensional compression and yield. In addition, formulas to aid in the design of RX implosions have been provided, and nonideal effects on RX adiabat shaping have been estimated.

TC6476a

Figure 101.6
Time evolution of the ablation velocities during the laser pulse's flattop for flat $\alpha = 3$ (dashed), decaying-shock–shaped (dotted), and type-2 relaxation-shaped (solid) implosions.

REFERENCES

1. W. K. Levedahl and J. D. Lindl, Nucl. Fusion **37**, 165 (1997).

2. M. M. Basko and J. Johner, Nucl. Fusion **38**, 1779 (1998).

3. M. C. Herrmann, M. Tabak, and J. D. Lindl, Nucl. Fusion **41**, 99 (2001).

4. A. Kemp, J. Meyer-ter-Vehn, and S. Atzeni, Phys. Rev. Lett. **86**, 3336 (2001).

5. R. Betti, K. Anderson, V. N. Goncharov, R. L. McCrory, D. D. Meyerhofer, S. Skupsky, and R. P. J. Town, Phys. Plasmas **9**, 2277 (2002).

6. K. Anderson and R. Betti, Phys. Plasmas **10**, 4448 (2003).

7. V. N. Goncharov, J. P. Knauer, P. W. McKenty, P. B. Radha, T. C. Sangster, S. Skupsky, R. Betti, R. L. McCrory, and D. D. Meyerhofer, Phys. Plasmas **10**, 1906 (2003).

8. K. Anderson and R. Betti, Phys. Plasmas **11**, 5 (2004).

9. L. J. Perkins, M. Tabak, J. Lindl, D. Bailey, J. Harte, A. Schmitt, S. Obenschain, and R. Betti, Bull. Am. Phys. Soc. **47**, 101 (2002).

10. K. Anderson, R. Betti, J. P. Knauer, and V. N. Goncharov, presented at the 34th Anomalous Absorption Conference, Gleneden Beach, OR, 2–7 May 2004.

11. J. H. Gardner, S. E. Bodner, and J. P. Dahlburg, Phys. Fluids B **3**, 1070 (1991).

12. S. E. Bodner *et al.*, Phys. Plasmas **7**, 2298 (2000).

13. L. Phillips *et al.*, Laser Part. Beams **17**, 225 (1999).

14. R. P. J. Town and L. J. Perkins, Lawrence Livermore National Laboratory, private communication (2003); M. Tabak, Lawrence Livermore National Laboratory, private communication (1987).

15. J. D. Lindl and W. C. Mead, Phys. Rev. Lett. **34**, 1273 (1975).

16. N. Metzler, A. L. Velikovich, and J. H. Gardner, Phys. Plasmas **6**, 3283 (1999).

17. N. Metzler *et al.*, Phys. Plasmas **9**, 5050 (2002).

18. N. Metzler *et al.*, Phys. Plasmas **10**, 1897 (2003).

19. T. J. B. Collins and S. Skupsky, Phys. Plasmas **9**, 275 (2002).

20. A. B. Iskakov *et al.*, Phys. Rev. E **61**, 842 (2000); E. Krousky *et al.*, Laser Part. Beams **18**, 87 (2000).

21. Laboratory for Laser Energetics LLE Review **98**, 106, NTIS document No. DOE/SF/19460-527 (2004). Copies may be obtained from the National Technical Information Service, Springfield, VA 22161.

22. R. Betti, K. Anderson, J. P. Knauer, T. J. B. Collins, R. L. McCrory, P. W. McKenty, and S. Skupsky, "Theory of Laser-Induced Adiabat Shaping in Inertial Confinement Fusion Implosions: The Relaxation Method," submitted to Physics of Plasmas.

23. K. Anderson, R. Betti, J. P. Knauer, and V. N. Goncharov, Bull. Am. Phys. Soc **49**, 210 (2004).

24. M. C. Richardson, P. W. McKenty, F. J. Marshall, C. P. Verdon, J. M. Soures, R. L. McCrory, O. Barnouin, R. S. Craxton, J. Delettrez, R. L. Hutchison, P. A. Jaanimagi, R. Keck, T. Kessler, H. Kim, S. A. Letzring, D. M. Roback, W. Seka, S. Skupsky, B. Yaakobi, S. M. Lane, and S. Prussin, in *Laser Interaction and Related Plasma Phenomena*, edited by H. Hora and G. H. Miley (Plenum Publishing, New York, 1986), Vol. 7, pp. 421–448.

25. T. R. Boehly, D. L. Brown, R. S. Craxton, R. L. Keck, J. P. Knauer, J. H. Kelly, T. J. Kessler, S. A. Kumpan, S. J. Loucks, S. A. Letzring, F. J. Marshall, R. L. McCrory, S. F. B. Morse, W. Seka, J. M. Soures, and C. P. Verdon, Opt. Commun. **133**, 495 (1997).